ENVIRONMENTAL RESEARCH
LETTERS

LETTER

The effect of African Easterly Wave suppression by periodicity on Atlantic tropical cyclones

Derrick K Danso[1,*], **Christina M Patricola**[1,2], **Emily Bercos-Hickey**[2] **and Christophe Lavaysse**[3]

[1] Department of the Earth, Atmosphere, and Climate, Iowa State University, Ames, IA, United States of America
[2] Climate and Ecosystem Sciences Division, Lawrence Berkeley National Laboratory, Berkeley, CA, United States of America
[3] Institut des Géosciences de l'Environnement, CNRS-UGA-INRAE-IRD-Grenoble INP, Grenoble, France
[*] Author to whom any correspondence should be addressed.

E-mail: ddanso@iastate.edu

Keywords: tropical cyclone, African Easterly Waves, Atlantic Ocean, environmental favorability, WRF model, periodicity

Supplementary material for this article is available online

OPEN ACCESS

RECEIVED
27 January 2025

REVISED
21 May 2025

ACCEPTED FOR PUBLICATION
19 June 2025

PUBLISHED
1 July 2025

Abstract

Research has shown that suppressing African Easterly Waves (AEWs) does not reduce basin-wide North Atlantic tropical cyclone (TC) frequency but can enhance TC environmental favorability. We investigated the AEW-TC relationship further by examining the effects of suppressing the two AEW periodicities individually on TC activity. Using regional model simulations, AEWs were prescribed or suppressed in the 2–6 d or 6–10 d ranges through the lateral boundary conditions. Seasonal TC frequency increased significantly when either AEW periodicity was suppressed, with a larger increase when the 2–6 d waves were suppressed. We also found that suppressing the 2–6 d waves increased mid-tropospheric moisture by up to 8%, as well as overall atmospheric instability, near the western coast of northern Africa. Furthermore, the convective disturbances that developed into TCs exhibited stronger rotation, increased ascending motion, and higher rainfall. Our results suggest that reduced 2–6 d AEW activity may trigger a more active TC season.

1. Introduction

Tropical cyclone (TC) genesis requires several conditions, including warm sea surface temperatures (SSTs), weak vertical wind shear (VWS), a moist mid-troposphere, and an initial disturbance (Emanuel 1988, Avila 1991, Landsea 1993, Frank and Ritchie 2001, Wong and Chan 2004, Lin *et al* 2013). In the tropical North Atlantic, the most common TC genesis precursor is African Easterly Waves (AEWs). AEWs are synoptic-scale disturbances that grow off of the baroclinic and barotropic instabilities of the African easterly jet (AEJ) and propagate westward across West Africa and over the Atlantic Ocean with a periodicity of 2–10 d (Carlson 1969, Burpee 1972, Diedhiou *et al* 1998). They typically form between 5° N and 30° N, primarily during the West African Monsoon season (May–October), although recent studies have shown they can occur year-round (Hollis *et al* 2024).

Previous studies have linked AEWs to TC genesis, with 60%–85% of Atlantic TCs developing from AEWs (Landsea 1993, Landsea *et al* 1998, Dieng *et al* 2017, Russell *et al* 2017). However, recent numerical model experiments designed to suppress AEWs indicate that AEWs are not necessary for maintaining seasonal basin-wide TC frequency (Patricola *et al* 2018, Danso *et al* 2022, Bercos-Hickey and Patricola 2023). For example, Patricola *et al* (2018) found no change in TC frequency when AEWs were filtered along the western coast of northern Africa using a 27 km resolution regional model with parameterized convection. Given the strong connection between AEWs and convection (Diedhiou *et al* 1999, Mekonnen *et al* 2006, Hsieh and Cook 2007, Schwendike and Jones 2010, Russell and Aiyyer 2020, Russell *et al* 2020) and the uncertainties of convection parameterization, Danso *et al* (2022) used a 3.5 km resolution model to conduct a similar experiment and reached the same conclusion. They also found that suppressing AEWs led to more favorable environmental conditions for TCs. Other studies have also shown that favorable environmental conditions have a stronger connection with TC frequency than AEWs (Caron and Jones 2012, Hoogewind *et al* 2020, Emanuel 2022).

AEWs occur in two distinct tracks along the AEJ near ∼11°N and ∼20°N (Diedhiou *et al* 1999, Pytharoulis and Thorncroft 1999, Chen *et al* 2008). Therefore, Bercos-Hickey and Patricola (2023) conducted numerical model experiments in which one type of AEW track was filtered while the other was maintained. Their results, consistent with previous studies (Patricola *et al* 2018, Danso *et al* 2022), showed that AEWs are not a limiting factor for TC genesis. They found that filtering either AEW track increased TC frequency, with the greatest increase occurring when the southern track was filtered. Despite the southern AEW track's greater efficiency in TC genesis (Goldenberg and Shapiro 1996, Chen 2006), suppressing it enhanced the large-scale environmental conditions favorable for TC formation.

AEWs are further classified into two regimes based on their periodicity: 2.5–6 d and 6–9 d, strongest at 700 hPa and between 950 and 850 hPa, respectively (de Félice *et al* 1993, Diedhiou *et al* 1998, 2002, Wu *et al* 2013). The filtering methods in previous studies by Patricola *et al* (2018), Danso *et al* (2022) and Bercos-Hickey and Patricola (2023) suppressed the full 2–10 d temporal spectrum of AEWs. Therefore, these studies did not separately account for the effects of filtering each AEW periodicity. While Bercos-Hickey and Patricola (2023) separately examined the southern and northern tracks—associated with the 2.5–6 d and 6–9 d AEWs, respectively—earlier studies have shown both wave periodicities occur north and south of the AEJ (Diedhiou *et al* 1999). Furthermore, since the northern and southern AEW tracks merge over the Atlantic into a single wave track (Hankes *et al* 2015, Duvel 2021), which is more favorable for TC genesis than either track alone (Chen and Liu 2014, Jonville *et al* 2024a), it is crucial to examine the AEW-TC relationship based on the different periodicities.

The objective of this study is to further investigate the AEW-TC relationship, specifically focusing on the effects of AEW suppression by periodicity. This study makes two primary and novel contributions to the understanding of Atlantic TC activity in relation to AEWs. First, we examine the response of Atlantic TC activity to the suppression of distinct AEW periodicity ranges. Second, we investigate the environmental conditions that influence the likelihood of different precursors developing into TCs. Given that only a small proportion of AEWs evolve into TCs (e.g. Thorncroft and Hodges 2001), and that different AEW periodicities and tracks exhibit varying efficiencies in initiating tropical cyclogenesis (e.g. Chen and Liu 2014), understanding the pre-genesis environment of TC precursors is essential for identifying the factors that enhance the potential for AEWs to transition into TCs. To achieve this, we used an ensemble of regional model simulations in which one of the two AEW periodicities was suppressed while the other was prescribed through the lateral boundary conditions. We then analyze statistical differences in TC activity, including TC frequency, intensity, translation speed, and lifetime. Additionally, we examine the environments associated with different TC precursors by analyzing the atmospheric conditions days prior to TC genesis.

2. Regional model simulations

The simulations were performed using version 4.2.2 of the Weather Research and Forecasting (WRF) model (Skamarock *et al* 2019). Initial and lateral boundary conditions, along with SST, were prescribed from the fifth-generation European Centre for Medium-Range Weather Forecasts (ECMWF) ReAnalysis (ERA5) dataset (Hersbach *et al* 2020). The model domain was chosen to leverage the flexibility of WRF, with the eastern lateral boundary placed around 15° W, just off the western edge of northern Africa (supporting information, figure S1). This configuration allows for the entry or suppression of AEWs into the model domain via the lateral boundary condition. The model was configured with a TC-permitting resolution of 27 km (Patricola *et al* 2016) and 45 vertical levels. Additionally, the following parameterization schemes were used: Kain–Fritsch scheme for cumulus clouds (Kain 2004), Purdue-Lin microphysics (Lin *et al* 1983), rapid radiative transfer model for general circulation models longwave and shortwave radiation (Iacono *et al* 2008), Yonsei University planetary boundary layer scheme (Hong *et al* 2006), revised MM5 surface scheme (Jiménez *et al* 2012), and the Noah land surface model (Chen and Dudhia 2001). The choice of model domain and parameterization schemes follows the setup of Patricola *et al* (2018) and Bercos-Hickey and Patricola (2023), which have been shown to realistically simulate TCs.

We first performed a control simulation in which AEWs were prescribed by ERA5 through the eastern lateral boundary. To investigate the effects of AEW suppression by periodicity, we conducted two experiments in which a band-stop filter was applied to all vertical levels of the variables in the eastern lateral boundary condition, between 5° S and 30° N, removing the 2.5–6 d and 6–9 d AEWs. In the first experiment (*'filtered (2–6 d)'*), we filtered the 2–6 d timescale, while in the second experiment (*'filtered (6–10 d)'*), we filtered the 6–10 d timescale to capture the full temporal range of AEWs. This approach is consistent with Patricola *et al* (2018) and Danso *et al* (2022), with the only difference being the filtered temporal ranges.

The simulations were performed for the 2020 hurricane season (1 May–30 November). This season was chosen due to the formation of several TCs near the western coast of northern Africa

(Klotzbach *et al* 2021), with the majority of these TCs originating from AEWs (Beven 2021). Ten ensemble members for the control and experimental simulations were generated by initializing the model on different dates (i.e. from 1 to 10 May). The model output was saved at 3 h intervals, and output from 1 June to 30 November was used for the analysis, with data before 1 June discarded as model spin-up. Simulated TCs were identified using the objective detection algorithm of Walsh (1997).

3. Results

3.1. Response of TC activity to AEW suppression by periodicity

We first examine the response of Atlantic TC activity to the filtering of different AEW time scales. There are considerable differences in the ensemble mean TC track densities across the simulations (figures 1(a)–(c)). For instance, suppressing the 2–6 d AEWs causes a shift in the location of peak TC activity near West Africa relatively westward (supporting information figure S2(c)). However, TC activity becomes more intense in the central main development region (from 50° W to 40° W and 10° N to 20° N) and in the Gulf of Mexico. The increased activity in the Gulf of Mexico increases the number of landfalling TCs (supporting information figure S3). Similar to suppressing the 2–6 d waves, filtering the 6–10 d AEWs increases TC activity in the Gulf of Mexico. Additionally, suppressing the 6–10 d AEWs also shifts peak TC activity near West Africa, though this shift is smaller compared to filtering the 2–6 d waves. This shift is seen as a reduction in TC track density north of 13° N and east of 25° W (supporting information figures S2(a) and (b)).

Suppressing either AEW periodicities leads to a statistically significant ($p < 0.05$) increase in the ensemble mean seasonal TC number, with values of 17, 20.7, and 19.7 TCs per season for the control simulation, the 2–6 d filtered experiment, and the 6–10 d filtered experiment, respectively (figure 1(d)). This result is consistent with earlier studies by Patricola *et al* (2018), Danso *et al* (2022), and Bercos-Hickey & Patricola (2023), which found that AEWs are not necessary to maintain the basin-wide frequency of TCs in the North Atlantic. We also found that suppressing both AEW periodicities resulted in slightly slower TCs on average, with a statistically significant difference in ensemble mean translation speed between the control and the 2–6 d filtered experiment (figure 1(e)). The AEW suppression experiments did not significantly change TC intensity, although the ensemble mean minimum sea level pressure was slightly lower when the 6–10 d AEWs were suppressed (figure 1(f)). Furthermore, suppressing both AEW periodicities did not significantly affect the average lifetime of TCs, with ensemble mean values of 4.9, 4.7, and 4.9 d for the control simulation, the 2–6 d filtered experiment, and the 6–10 d filtered experiment, respectively (figure 1(g)).

3.2. Response of wave activity to suppression by periodicity

To compare the effects of filtering different AEW periodicities, we performed a wavelet decomposition of the meridional wind east of 20° W at low levels (950 hPa) and AEJ levels (700 hPa) to highlight the frequency windows active during the simulation period. The power spectra at these levels help identify disturbances near the west coast of northern Africa (Pytharoulis and Thorncroft 1999, Gu *et al* 2004, Jonville *et al* 2024b). Figures 2(a)–(c) show the mean wavelet power of the ensemble-averaged 700 hPa meridional wind from 0° to 15° N, where the southern AEW track is located. In the control, most wave activity is found in the 2–6 d range, peaking between August and September (figure 2(a)). Some wave activity is also observed in the 6–10 d range, although its power spectrum is lower than that of the 2–6 d range. Filtering AEWs in the 2–6 d range removes wave activity in that frequency range, although some wave activity remains overlapping the two filtered regimes (3.5–10 d) (figure 2(b)). The remaining wave activity seems to have intensified, which could suggest that the presence of 2–6 d waves dampens the background environmental conditions in which other wave periodicities grow. The previous work of Bercos-Hickey and Patricola (2023) supports this idea, as they found that the suppression of the southern AEW track—typically dominated by 2–6 d waves—enhanced the environmental conditions favorable for TC development. This could explain the intensification of the 6–10 d waves when the 2–6 d waves are filtered. The reduction in the filtered range can also be seen by calculating the difference in the wavelet power density between the 2–6 d filtering experiment and the control (supporting information figure S4). In contrast, filtering the 6–10 d range almost entirely removes wave activity in that band at 700 hPa, leaving only the wave activity in the 2–6 d range (figure 2(c)). A similar result is observed when the wavelet power is computed between 15° N and 30° N, where the northern AEW track is located (not shown).

The mean power spectrum of the ensemble-averaged 950 hPa meridional wind from 15° N to 30° N is also assessed (figures 2(d)–(f)). In the control simulation, wave activity is present in both temporal bands, although the 2–6 d range appears to be dominant once again (figure 2(d)). Filtering AEWs in the 2–6 d range substantially removes wave activity in that band (figure 2(e)). Similarly, filtering AEWs in the 6–10 d range removes nearly all wave activity in that band (figure 2(f)), although some wave activity remains overlapping the two periodicities in the 4–8 d range. As shown in figure 1(d), filtering either

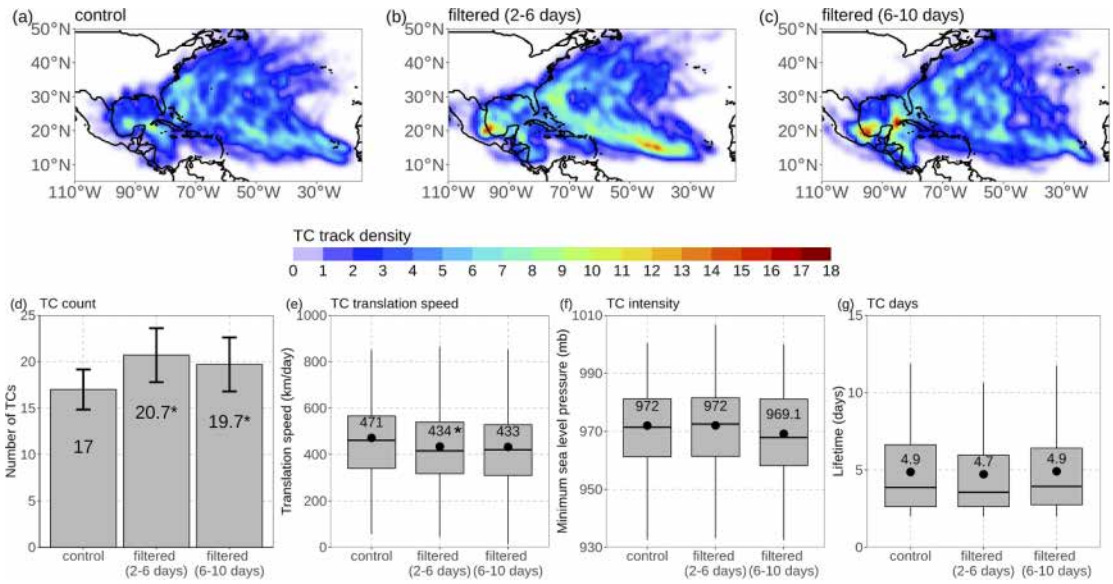

Figure 1. (a)–(c) Ensemble mean TC track densities (TCs per season) for the WRF (a) control simulation, (b) 2–6 d filtered AEW suppression experiment, and (c) 6–10 d AEW suppression experiment. (d)–(g) Simulated (d) ensemble mean Atlantic TC frequency, (e) TC translation speed (km d^{-1}), (f) TC intensity (hPa), and (g) TC lifetime (days). Both the black dots and the numbers represent the ensemble mean value. The error bars represent the variation among the ten ensemble members. An asterisk (*) next to a number indicates a statistically significant difference from the control simulation (p-value < 0.05).

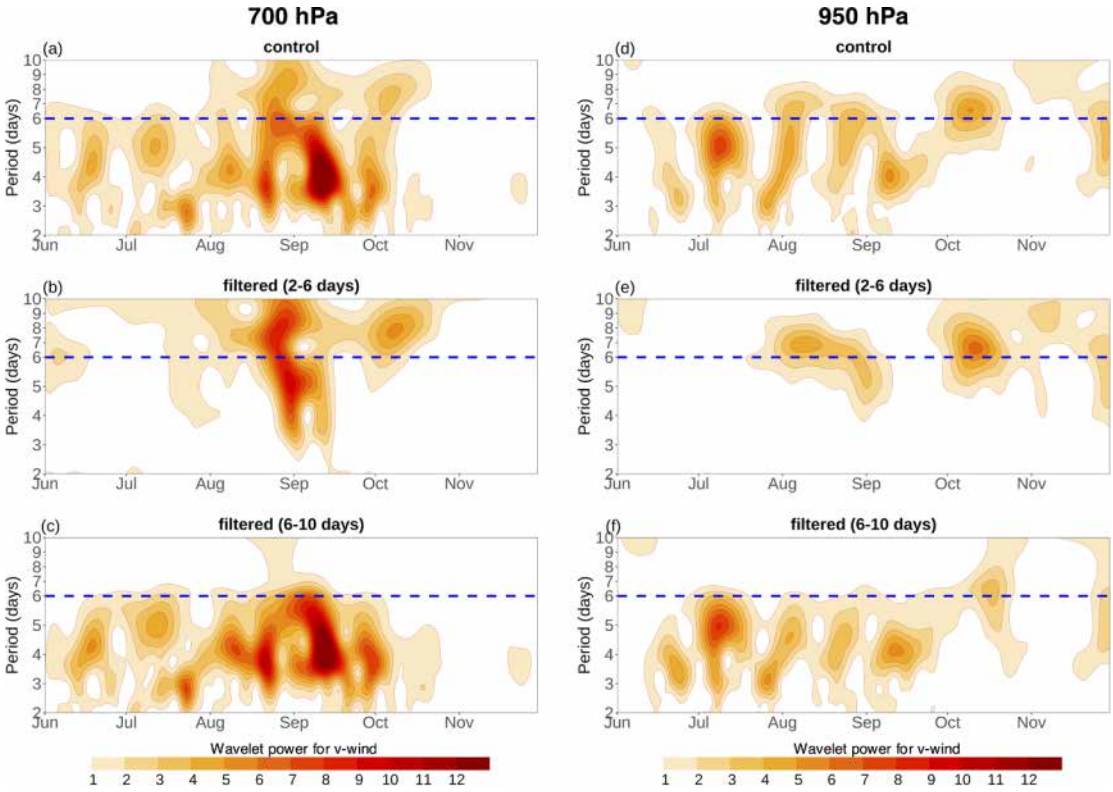

Figure 2. Ensemble mean wavelet power density ($m^2 s^{-3}$) of meridional wind between 20° W and 15° W at (a)–(c) 700 hPa averaged from 0° to 15° N and (d)–(f) 950 hPa averaged from 15° N to 30° N for the WRF control simulation (top row), the 2–6 d filtered AEW suppression experiment (middle row), and the 6–10 d AEW suppression experiment (bottom row) from June to November 2020. The dotted blue line represents the division between the 2–6 d and 6–10 d periodicities. Note the different color scales for the 700 and 950 hPa power densities.

of the AEW periodicities does not reduce TC genesis. This is supported by the previous work of Patricola *et al* (2018) and Danso *et al* (2022), both of whom noted that, in the absence of AEWs, other convective disturbances may serve as precursors for TC genesis. Therefore, the additional wave periodicities that

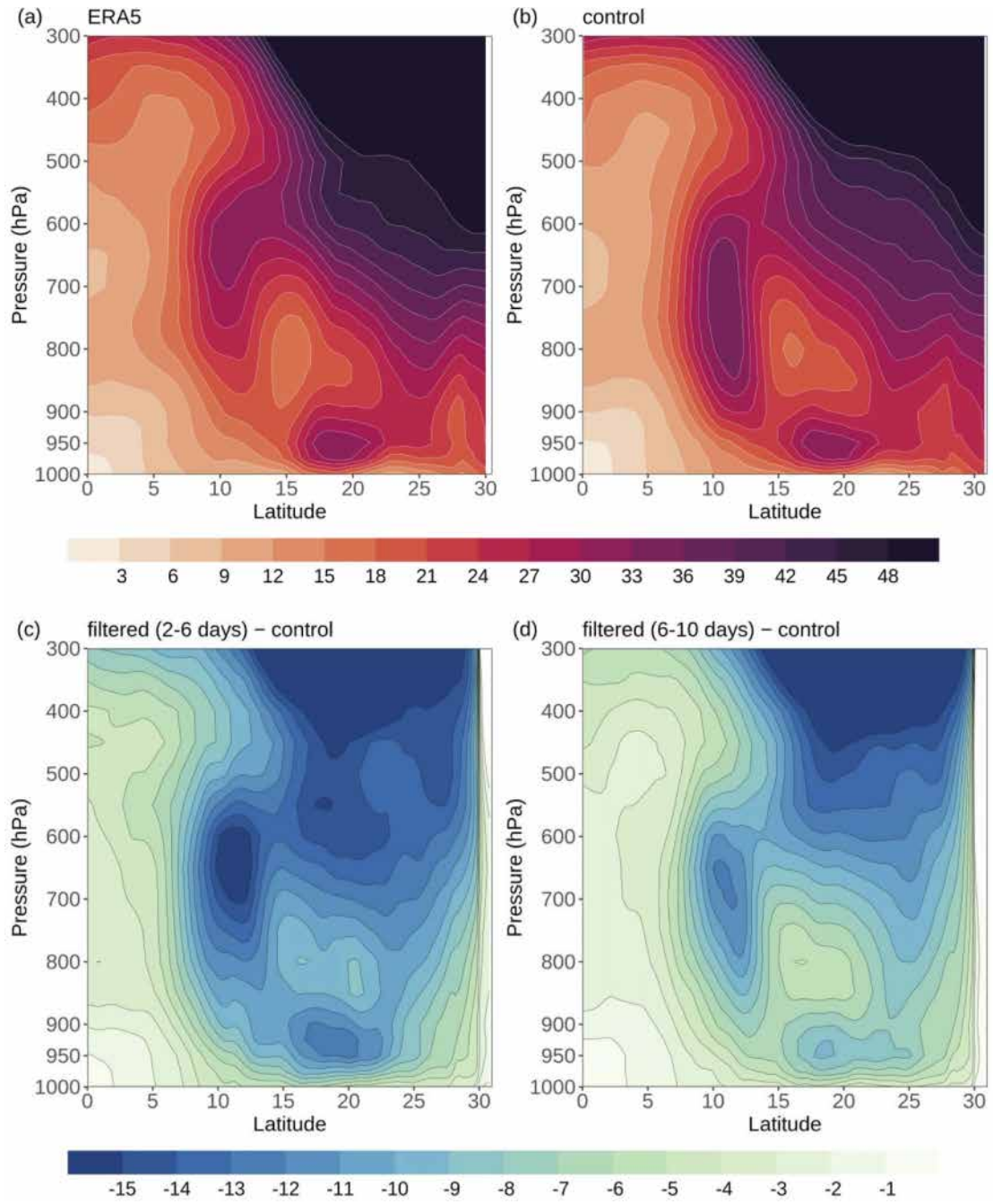

Figure 3. (a), (b) Vertical cross section of eddy kinetic energy (m^2s^{-2}) averaged between 20° W and 15° W for (a) ERA5 and (b) the ensemble mean WRF control simulation. (c), (d) The ensemble mean eddy kinetic energy for the (c) 2–6 d filtered experiment minus the control and (d) 6–10 d filtered experiment and the control.

appear in the 0°–15° N (i.e. 3.5–10 d) and 15° N to 30° N (i.e. 4–8 d) wavelet spectra when filtering the 2–6 d and 6–10 d bands, respectively, may not necessarily be AEWs but could instead represent other tropical disturbances that develop in the region, which could also serve as precursor disturbances for TC genesis. Therefore, our results suggest that, in the absence of the 2–6 d waves, the 6–10 d and other wave periodicities may provide some of the precursor disturbances for TC genesis, and vice versa. Additionally, it is important to note that both main AEW periodicities are present in both the northern and southern AEW tracks.

To quantify the vertical structure of AEW activity we used the seasonal mean eddy kinetic energy (EKE) (figure 3). Previous studies have shown that EKE is a useful measure of AEW activity (Hsieh and Cook 2007, Diaz and Aiyyer 2013, Russell *et al* 2017). To assess how well the WRF model reproduced AEW activity in the control simulations, we estimated EKE using ERA5 for the same time window analyzed in the WRF simulations. ERA5 shows stronger EKE in

the regions of the two AEW tracks (figure 3(a)), with intense activity between 700 hPa and 600 hPa around 8° N–13° N corresponding to the southern track, and a second area of intense activity between the surface and 900 hPa around 16° N to 23° N, corresponding to the northern track. The ensemble averaged EKE from the WRF control simulation captures both AEW tracks (figure 3(b)). However, the core of the southern AEW track extends from about 850 hPa to 600 hPa and shifts slightly northward. Overall, AEW activity is reasonably well captured in the WRF model control simulations.

Suppressing AEWs in either the 2–6 d or 6–10 d range decreases EKE (figures 3(c) and (d)), particularly in the regions of the two wave tracks. However, there are notable differences in the magnitude of this reduction. Suppressing AEWs in the 2–6 d range leads to a larger decrease in EKE compared to suppressing AEWs in the 6–10 d range. In the experiment with 2–6 d AEWs suppressed, EKE decreases in both the northern and southern tracks, though slightly more in the southern track. Similarly, suppressing AEWs in the 6–10 d range decreases EKE in both tracks, with no distinct difference in the magnitude of the reduction. The larger EKE decrease when suppressing the 2–6 d AEWs indicates that most wave activity occurs in this range, as shown in the wavelet power spectrum (figure 1). Additionally, the decreased EKE in both AEW tracks suggests the presence of both AEW periodicities in the northern and southern tracks. We note that suppressing AEWs of either periodicity does not affect the location or size of the AEJ near the western coast of northern Africa, though its intensity slightly decreases in both filters (supporting information figure S5).

3.3. TC precursors and associated atmospheric conditions

We now examine the origins of the precursors that develop into TCs by analyzing Hovmöller diagrams of rainfall rate and 700 hPa relative vorticity averaged over 8° N–23° N for one single ensemble member and the ensemble mean in the control simulation and experiments (figure 4 and supporting information figure S6) and the TC genesis location and times (green triangles). A TC that originates from an AEW will typically show a positive vorticity signal and/or a westward-propagating rainfall track (Tyner and Aiyyer 2012, Russell and Aiyyer 2020, Russell *et al* 2020) from around 15° W (where the eastern lateral boundary is) to the location of TC genesis. In the control simulation of the single ensemble member, we found that some TCs appear to originate from AEWs, while others do not (figure 4(a) and supporting information figure S6). This suggests that AEWs are not the sole source of TC precursors, and other convective disturbances may also trigger TC genesis. Convective disturbances can originate within the Intertropical Convergence Zone (ITCZ) through wave-breaking, a process first observed in satellite data during the study of Tropical Storm Anna (Agee 1972). These wavelike disturbances, independent of AEWs, can amplify and break, potentially forming TC vortices. Subtropical pressure systems may also foster convective environments favorable for TC genesis (Pérez-Alarcón *et al* 2021). Furthermore, idealized simulations show that moist convection can spontaneously self-aggregate into clusters, which could in turn trigger TC genesis (Muller and Held 2012, Wing *et al* 2017).

When the 2–6 d waves are suppressed, some TCs exhibit a clear AEW origin, while others do not (figure 4(b) and supporting information figure S6). The TCs with an AEW origin are likely associated with the 6–10 d waves, while the others may result from different convective disturbances. Similarly, when the 6–10 d waves are suppressed, some TCs originate from AEWs, likely associated to the 2–6 d waves, while others still generate from non-AEW sources (figure 4(c) and supporting information figure S6). This result shows that in the absence of one periodicity, there are TCs with AEW origins from the other periodicity, as well as non-AEW TCs.

In the ensemble mean (figure 4(d)), we found a relatively higher number of TC genesis clusters that appear to have originated from AEWs in similar locations and times in the control simulation (for example, near 20° W around 7 and 12 September) compared to both AEW filtered experiments. This suggests that TCs developing from AEWs in the control simulation typically form around the same locations and times across the ensemble members, which makes sense given that each ensemble member has the same AEWs prescribed from the lateral boundary condition. Like the control, there is a similar cluster of TC genesis near 20° W and around September 12 in the 6–10 d filtered experiment, which indicates that those TCs likely developed from the same 2–6 d AEW in the different ensembles. In contrast, while there are fewer TC genesis clusters, the genesis of TCs appears to be more spatially and temporally dispersed when filtering one kind of AEW, particularly in the 2–6 d filtered experiment (figures 4(e) and (f)). As shown in previous studies, AEWs can interact with different convective systems to influence TC activity (Mekonnen *et al* 2006, Enyew and Mekonnen 2021). Since evidence of TC genesis from AEWs is found in all individual ensemble members when filtering one kind of AEW periodicity, it is possible that some of the TC genesis events that do not cluster in the Hovmöller diagrams could still have AEW origins. However, convective disturbances in the WRF model ensembles may interact with AEWs, modifying

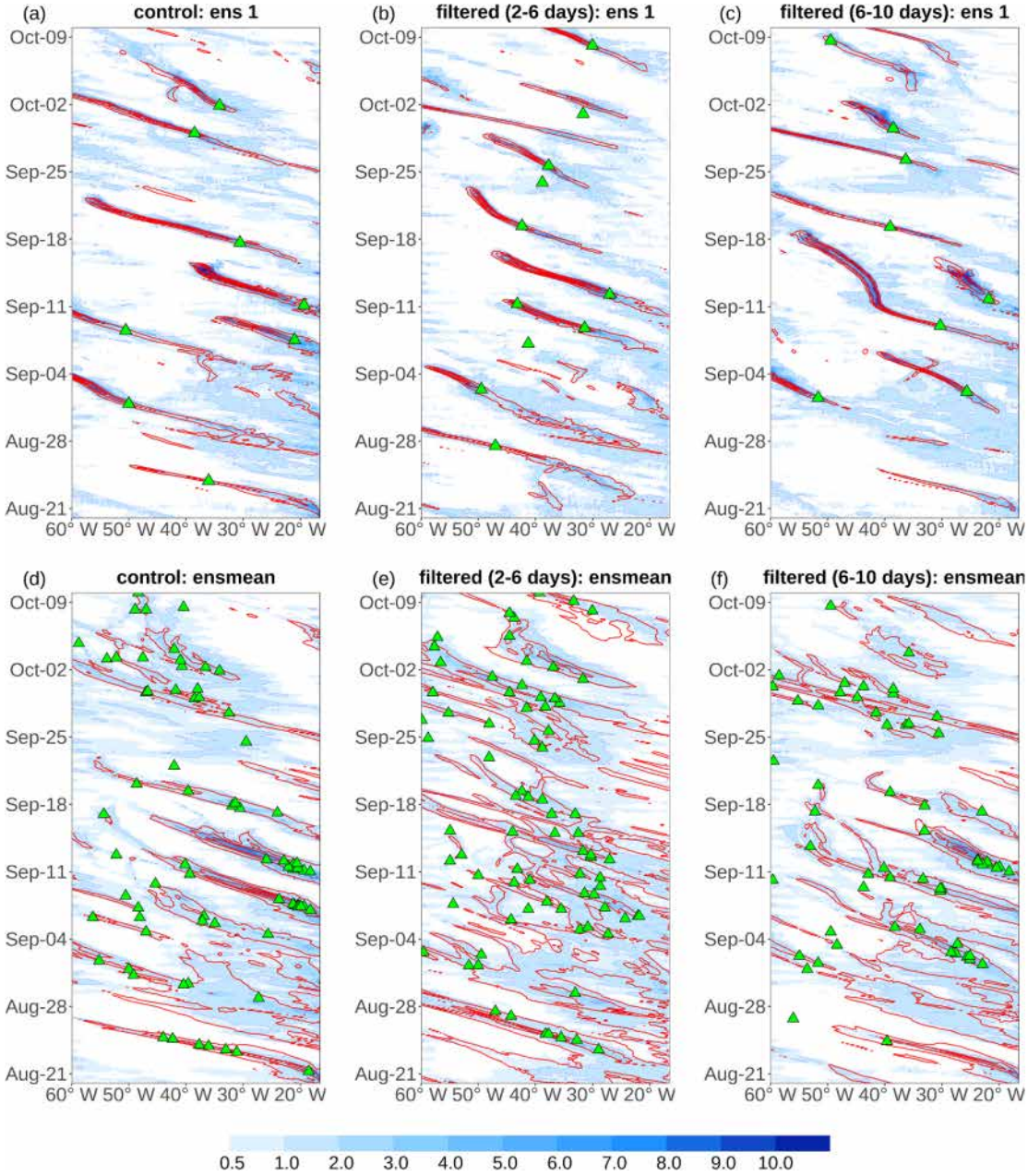

Figure 4. Hovmöller diagrams of rainfall rate (mm h^{-1}) (shading) and positive relative vorticity at 700 hPa (contours) averaged between 8° N–23° N from (a)–(c) an individual ensemble member and (d)–(f) the 10-member ensemble mean of the control simulation and 2–6 d and 6–10 d AEW filtering experiments. The green triangles indicate TC genesis location and time.

the locations and timing of TC genesis when filtering one kind of AEW periodicity.

To better understand the atmospheric conditions associated with TC formation in the absence of either AEW periodicity, we also analyze composites of 850 hPa relative vorticity, integrated vertical velocity integrated over all levels, and rainfall rate of the disturbances leading up to TC formation. For this analysis, we define a reference region with a 2000 km radius, centered on the location of the TC at the time of genesis. To isolate the TC precursors, we limit our analysis to the 72–12 h prior to genesis. While we did not explicitly track individual disturbances, an examination of several TC cases indicates that the 2000 km reference radius is sufficiently large to capture the primary activity of the disturbances up to 72 h before genesis (supporting information figure S7). To focus primarily on TCs that likely formed from AEWs, we limited our analysis to only TCs that formed east of 60° W.

The sum of the positive 850 hPa relative vorticity from 72 to 12 h before TC genesis, averaged across all TCs for the control and experiments, is shown in figures 5(a)–(c). Relative vorticity at 850 hPa is greater when suppressing AEWs in the 2–6 d range, compared to both the control and when suppressing the 6–10 d AEWs. A closer look at individual hours prior to TC genesis also shows this pattern

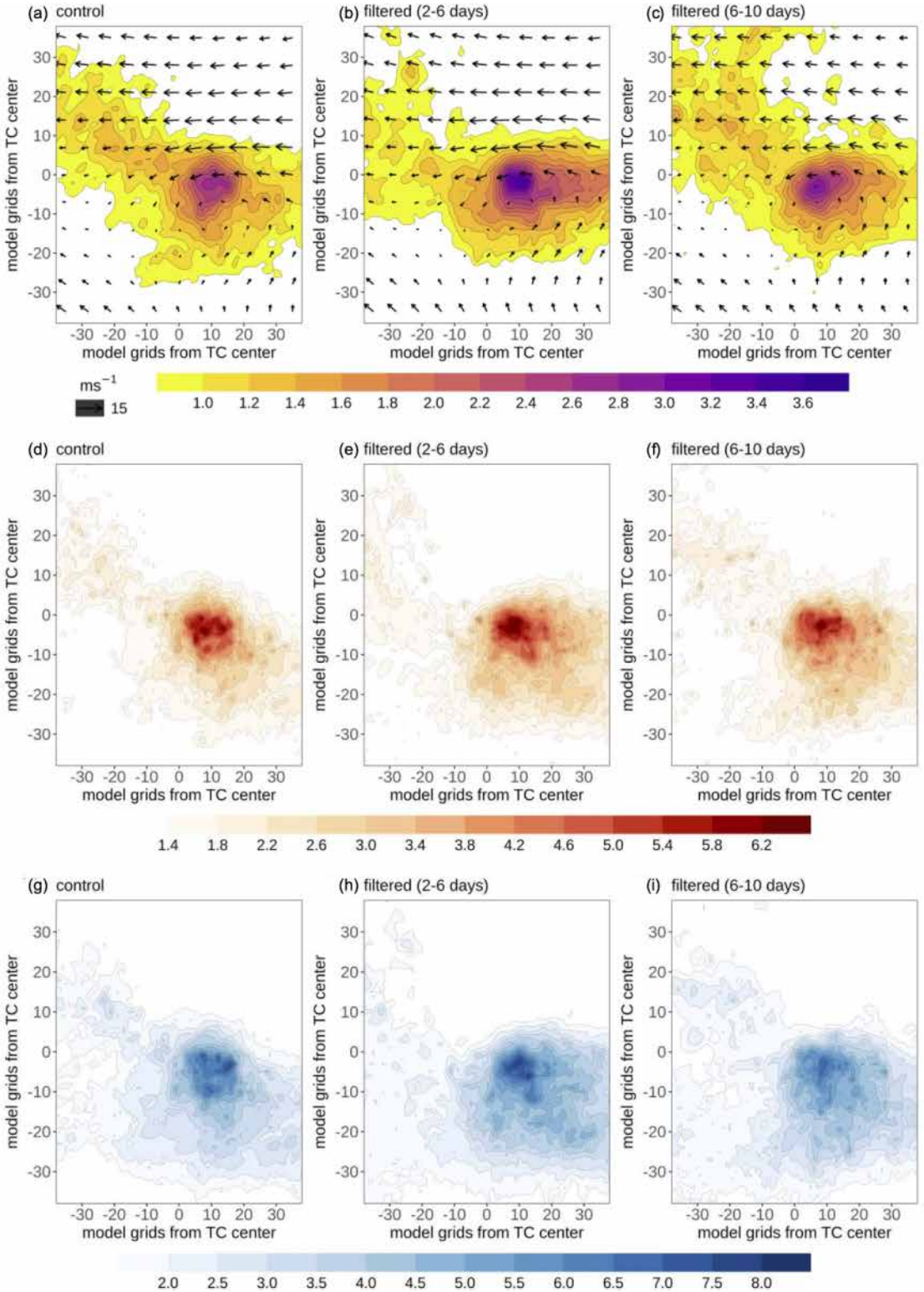

Figure 5. Simulated sum of (a)–(c) positive 850 hPa relative vorticity (10^{-4} s^{-1}), (d)–(f) vertical velocity integrated over all levels (m s^{-1}), and (g)–(i) rainfall rate (mm h^{-1}) from 72 to 12 h (at 12 h intervals) before TC genesis, averaged across all TCs formed east of 60° W and all ensembles. The arrows in (a)–(c) represent the composite mean wind vectors. The number (percentage) of TCs formed east of 60° W across all ensembles are 90 (53%), 107 (52%), and 89 (45%) for the control, 2–6 d filtered experiment, and 6–10 d filtered experiment, respectively. The values are composited for all TCs within a 2000 km × 2000 km box centered on the TC location at the time of genesis. This is zoomed to 1000 km × 1000 km.

(supporting information figure S7). This suggests that, in the absence of the 2–6 d AEWs, other disturbances must be rotating more strongly to eventually develop into TCs. The same analysis with integrated vertical velocity (figures 5(d)–(f) and supporting information figure S8) and mid-tropospheric vertical velocity (not shown) yields similar results, indicating stronger convection is present within the

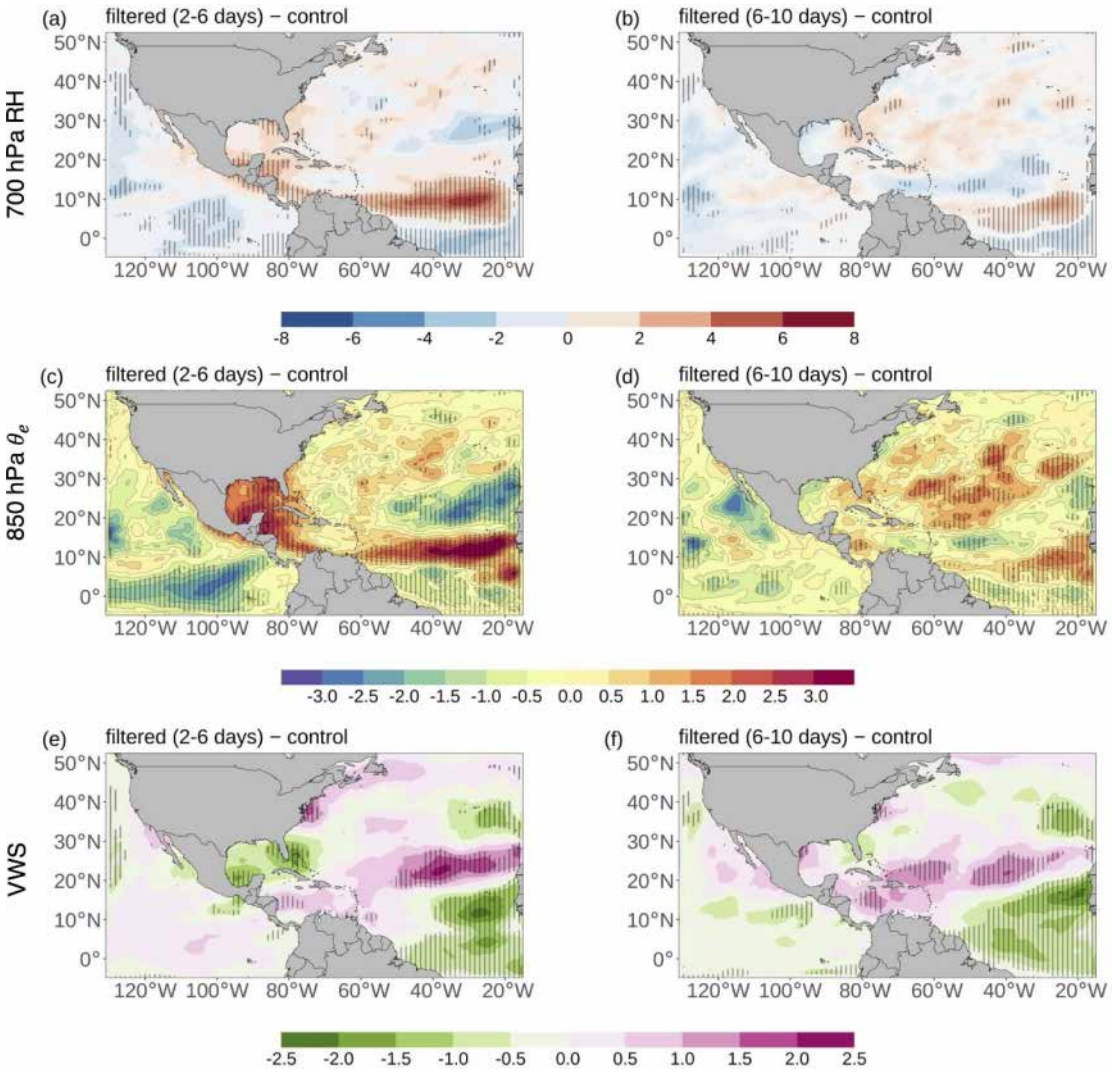

Figure 6. (a), (b) Simulated ensemble mean time-averaged 700 hPa relative humidity (%) for (a) the 2–6 d filtered experiment minus the control, and (b) the 6–10 d filtered experiment minus the control. (c), (d) Same as (a), (b), but for 850 hPa equivalent potential temperature (K). (e), (f) Same as (a), (b), but for vertical wind shear between 850 and 200 hPa (m s^{-1}). Hatches denote areas where the difference between the experiments and the control is statistically significant (p-value < 0.05) based on a grid-cell-specific two-sample t-test.

disturbances that develop into TCs when the 2–6 d AEWs are suppressed. Finally, an examination of rainfall during the disturbance phase shows a comparable result (figures 5(g)–(i) and supporting information figure S9), with higher rainfall rates when the 2–6 d AEWs are suppressed. The stronger rotation, convection, and higher rainfall in the disturbances that generate TCs without the 2–6 d AEWs likely suggest that these disturbances may need to reach a more mature vortex phase before triggering TC genesis. It is also possible that the presence of the 2–6 d AEWs weakens the background conditions for pre-TC genesis, and therefore, their absence enhances such conditions, potentially supporting the development of other wave periodicities. This is because previous research has shown that suppressing the south AEW track, which is dominated by the 2–6 d periodicity, improves large-scale environmental conditions that favor TC development (Bercos-Hickey and Patricola 2023). Additionally, previous research has shown that rain rate and low-to-mid-level tropospheric relative vorticity are among the best predictors of TC genesis in the North Atlantic (Peng *et al* 2012). Thus, higher values of these variables in the 2–6 d filtered experiment could support the interpretation that the presence and absence of the 2–6 d waves respectively weaken and strengthen the background conditions for TC genesis.

3.4. Mean state atmospheric conditions

Next, we examine the differences in mean state atmospheric conditions—relative humidity (RH), equivalent potential temperature (θ_e), and the 850–200 hPa VWS—between the experiments and the control simulation (figure 6). When suppressing the 2–6 d AEWs, we found statistically significant (p-value < 0.05) positive anomalies in 700 hPa RH, up to 8%, particularly near the western coast of northern Africa and

in the Gulf of Mexico (figure 6(a)). The areas with the greatest positive anomalies correspond to locations with the highest TC track densities (figure 1(b)). Similar results were also found at 600 hPa (supporting information figure S10) as well as in the total column precipitable water (supporting information figure S11), which shows a strong spatial correlation with the mid-tropospheric moisture (figures 6(a) and (b)). In contrast, both positive and negative RH anomalies are found near the western coast of northern Africa and in the Gulf of Mexico when suppressing the 6–10 d AEWs, though the positive anomalies are much weaker than those seen when suppressing the 2–6 d AEWs (figure 6(b)). This suggests that suppressing the 2–6 d AEWs drives an increase in mid-tropospheric moisture, which increases environmental favorability and may partly explain the stronger relative vorticity and convection found in figure 5. This finding is consistent with Núñez Ocasio *et al* (2024), who conducted moisture sensitivity experiments and found increased vertical motion and relative vorticity within an easterly wave that developed into a TC in a moister environment compared to a drier case. They also noted that higher environmental moisture reduced the translation speed of the disturbance. While their study focused only on the disturbance phase, their results align with our finding of decreased TC translation speed when suppressing the 2–6 d AEWs.

The moisture signature and overall favorability of the region when suppressing the 2–6 d AEWs is also evident in the 850 hPa θ_e (figure 6(c)). As shown in previous studies, the 850 hPa θ_e in the environment of AEWs that develop into TCs is higher than in non-developing AEWs (Núñez Ocasio *et al* 2021). Since there are considerably more AEWs in the 2–6 d range than in the 6–10 d range (figure 2), there is also a greater likelihood of more non-developing AEWs in the former, given that only a small fraction of AEWs develop into TCs (Pasch and Avila 1994, Thorncroft and Hodges 2001). Therefore, it is possible the seasonal mean 850 hPa θ_e is lower in the 6–10 d filtered experiment (figure 6(d)) due to the relatively higher number of non-developing 2–6 d AEWs. The environmental favorability is further evident in the indicators such as the convective available potential energy, which show relatively higher value in the eastern main development region in the 2–6 d filtered experiment (supporting information figure S12).

We also found that suppressing both AEW periodicities weakened the VWS near the western coast of northern Africa (figures 5(e) and (f)). This may be due to a weakening of the tropical easterly jet, which is observed in the suppression experiments (supporting information figure S13), a result also noted in the suppression experiments of Bercos-Hickey and Patricola (2023). Additionally, there is a weakening of the zonal wind flow within the AEJ in both suppression experiments, with the weakening being slightly more pronounced when AEWs are suppressed in the 2–6 d range (supporting information figure S13). This could partly explain the slower translation speeds of the TCs in the suppression experiments, with the decrease in speed being statistically significant when the 2–6 d AEWs are suppressed.

4. Summary and conclusions

The most common type of TC precursor disturbance in the tropical North Atlantic is AEWs. However, recent studies have shown that AEWs are not necessary for maintaining the basin-wide seasonal frequency of TCs in the North Atlantic (Patricola *et al* 2018, Danso *et al* 2022, Bercos-Hickey and Patricola 2023) and that large-scale environmental conditions are more strongly correlated with seasonal TC activity (Caron and Jones 2012, Emanuel 2022). In this study, we further investigated the AEW-TC relationship by examining how the suppression of the two AEW periodicities individually affected North Atlantic TC activity in 2020, using a suite of TC-permitting simulations. To do this, we generated an ensemble of TC-permitting regional model simulations in which AEWs were prescribed through the lateral boundary conditions (control), filtered in the 2–6 d range, or filtered in the 6–10 d range.

From the suppression experiments, we found that in the absence of 2–6 d AEWs, other wave periodicities strengthen and may provide some of the precursor disturbances that generate TCs. Suppressing AEWs in the 2–6 d range resulted in a greater decrease in EKE compared to suppressing AEWs in the 6–10 d range, suggesting that most AEW activity occurs in the 2–6 d range. EKE decreased in both the southern and northern AEW tracks in both experiments, indicating that both AEW periodicities are present in these tracks. Additionally, we found that suppressing either AEW periodicity resulted in a statistically significant increase in seasonal TC frequency, with the largest increase occurring when the 2–6 d waves were suppressed. This increase in TC frequency is consistent with the findings of Bercos-Hickey and Patricola (2023). Furthermore, suppressing both AEW periodicities resulted in a decrease in mean TC translation speed, with a statistically significant reduction in the 2–6 d filtered experiment.

By examining the large-scale environmental conditions, we found that suppressing the 2–6 d AEWs resulted in statistically significant positive anomalies in 700 hPa RH, up to 8%, particularly near the western coast of northern Africa and the Gulf of Mexico, corresponding to areas with the highest TC track densities. Similarly, we observed statistically significant positive anomalies in 850 hPa θ_e in the same regions, indicating increased atmospheric instability. This enhanced environmental favorability may

partly explain the higher TC frequency when the 2–6 d waves are suppressed. We also found that relative vorticity and convective activity prior to TC formation were stronger when the 2–6 d waves were suppressed. Additionally, rainfall during the disturbance phase of TCs was higher, suggesting that precursors may need to reach a more mature stage to trigger TC genesis in the absence of the 2–6 d waves, with this maturity facilitated by more favorable environmental conditions.

Both this study and previous work (Danso *et al* 2022, Bercos-Hickey and Patricola 2023) have demonstrated that the absence of AEWs results in increased environmental favorability for TC genesis. In our case, we have shown that the increase in environmental favorability is greater in the absence of the 2–6 d waves. This suggests that potential future changes in AEWs (e.g. Skinner and Diffenbaugh 2014) could lead to modifications in the large-scale environment that influence TC activity. Given the role that tropical waves play in organizing convection by modulating moisture and creating convergence zones, their absence may lead to an accumulation of convective energy over time. This accumulated energy could increase atmospheric instability, which may trigger a more active TC season when other environmental conditions are favorable. These interactions remain understudied and could further enhance our understanding of the AEW-TC relationship. Therefore, it is important to investigate exactly how the absence of AEWs creates such favorable conditions in the large-scale environment and how their presence may dampen background conditions important for pre-TC genesis in future work. Additionally, future work could explore how the inclusion of air–sea interactions in a coupled model framework might modify the influence of AEWs on TC development, particularly in terms of AEW evolution and subsequent development into TCs.

In the broader context of environmental science, our results are important for understanding the potential impacts of climate variability and change on regional climates. The study's findings—highlighting how AEWs influence environmental factors such as atmospheric instability, moisture availability, and vorticity—are particularly relevant to regional climate modeling, especially in improving seasonal and sub-seasonal forecasting of extreme weather events. For instance, the increased environmental favorability for TC genesis simulated in the absence of AEWs may inform predictions on how shifts in these disturbances, and associated changes in TCs, could affect ecosystems, coastal areas, and agriculture, particularly in vulnerable regions like the Caribbean and along the US East and Gulf coasts. These can also help refine climate projections and inform strategies for mitigating the socio-environmental impacts of extreme weather events.

Data availability statement

The output of the WRF model simulations is archived on the NERSC High Performance Storage System (HPSS) storage system and available from the authors upon reasonable request.

The data that support the findings of this study are openly available at the following URL/DOI: https://cds.climate.copernicus.eu/datasets, https://docs.nersc.gov/filesystems/archive/.

Acknowledgment

This material is based upon work supported by the U.S. Department of Energy, Office of Science, Office of Biological and Environmental Research (BER), Earth and Environmental Systems Modeling (EESM) Program, under Award Number DE-AC02-05CH11231. This research used resources of the National Energy Research Scientific Computing Center (NERSC), a Department of Energy Office of Science User Facility using NERSC Award BER-ERCAPm1517 for 2024. The authors thank three anonymous reviewers for their constructive comments that helped improve the manuscript.

References

Agee E M 1972 Note on ITCZ wave disturbances and formation of Tropical Storm Anna *Mon. Weather Rev.* **100** 733–7

Avila L A 1991 Atlantic Tropical systems of 1990 *Mon. Weather Rev.* **119** 2027–33

Bercos-Hickey E and Patricola C M 2023 The effects of African Easterly Wave suppression by wave track on Atlantic Tropical cyclones *Geophys. Res. Lett.* **50** e2023GL105491

Beven J L 2021 The 2020 Atlantic Hurricane season: the most active season on record *Weatherwise* **74** 33–43

Burpee R 1972 The origin and structure of easterly waves in the lower Troposphere of North Africa *J. Atmos. Sci.* **29** 77–90

Carlson T N 1969 Some remarks on African disturbances and their progress over the Tropical Atlantic *Mon. Weather Rev.* **97** 716–26

Caron L-P and Jones C G 2012 Understanding and simulating the link between African Easterly Waves and Atlantic tropical cyclones using a regional climate model: the role of domain size and lateral boundary conditions *Clim. Dyn.* **39** 113–35

Chen F and Dudhia J 2001 Coupling an advanced land surface-hydrology model with the Penn State-NCAR MM5 modeling system. Part I: model implementation and sensitivity *Mon. Weather Rev.* **129** 569–85

Chen S-H and Liu Y-C 2014 The relation between dry vortex merger and tropical cyclone genesis over the Atlantic Ocean *J. Geophys. Res. Atmos.* **119** 11641–61

Chen T-C 2006 Characteristics of African Easterly Waves depicted by ECMWF reanalyses for 1991–2000 *Mon. Weather Rev.* **134** 3539–66

Chen T-C, Wang S-Y and Clark A J 2008 North Atlantic hurricanes contributed by African Easterly Waves North and south of the African easterly jet *J. Clim.* **21** 6767–76

Danso D K, Patricola C M and Bercos-Hickey E 2022 Influence of African Easterly Wave suppression on Atlantic Tropical cyclone activity in a convection-permitting model *Geophys. Res. Lett.* **49** e2022GL100590

de Félice P, Viltard A and Oubuih J 1993 A synoptic-scale wave of 6–9 day period in the Atlantic Tropical troposphere during summer 1981 *Mon. Weather Rev.* **121** 1291–8
Diaz M and Aiyyer A 2013 Energy dispersion in African Easterly Waves *J. Atmos. Sci.* **70** 130–45
Diedhiou A, Janicot S, Viltard A and de Felice P 1998 Evidence of two regimes of easterly waves over West Africa and the tropical Atlantic *Geophys. Res. Lett.* **25** 2805–8
Diedhiou A, Janicot S, Viltard A and de Felice P 2002 Energetics of easterly wave disturbances over West Africa and the tropical Atlantic: a climatology from the 1979–95 NCEP/NCAR reanalyses *Clim. Dyn.* **18** 487–500
Diedhiou A, Janicot S, Viltard A, de Felice P and Laurent H 1999 Easterly wave regimes and associated convection over West Africa and tropical Atlantic: results from the NCEP/NCAR and ECMWF reanalyses *Clim. Dyn.* **15** 795–822
Dieng A L, Sall S M, Eymard L, Leduc-Leballeur M and Lazar A 2017 Trains of African Easterly Waves and their relationship to tropical cyclone genesis in the Eastern Atlantic *Mon. Weather Rev.* **145** 599–616
Duvel J-P 2021 On vortices initiated over West Africa and their impact on North Atlantic Tropical cyclones *Mon. Weather Rev.* **149** 585–601
Emanuel K 1988 The Maximum intensity of Hurricanes *J. Atmos. Sci.* **45** 1143–55
Emanuel K 2022 Tropical cyclone seeds, transition probabilities, and genesis *J. Clim.* **35** 1–28
Enyew B D and Mekonnen A 2021 The interaction between African Easterly Waves and different types of deep convection and its influence on Atlantic Tropical cyclones *Atmosphere* **13** 5
Frank W M and Ritchie E A 2001 Effects of vertical wind shear on the intensity and structure of numerically simulated hurricanes *Mon. Weather Rev.* **129** 2249–69
Goldenberg S B and Shapiro L J 1996 Physical mechanisms for the association of El Niño and West African rainfall with Atlantic major hurricane activity *J. Clim.* **9** 1169–87
Gu G, Adler R F, Huffman G J and Curtis S 2004 African Easterly Waves and their association with precipitation *J. Geophys. Res. Atmos.* **109** D04101
Hankes I, Wang Z, Zhang G and Fritz C 2015 Merger of African Easterly Waves and formation of Cape Verde storms *Q. J. R. Meteorol. Soc.* **141** 1306–19
Hersbach H *et al* 2020 The ERA5 global reanalysis *Q. J. R. Meteorol. Soc.* **146** 1999–2049
Hollis M A, McCrary R R, Stachnik J P, Lewis-Merritt C and Martin E R 2024 A global climatology of tropical easterly waves *Clim. Dyn.* **62** 2317–32
Hong S-Y, Noh Y and Dudhia J 2006 A new vertical diffusion package with an explicit treatment of entrainment processes *Mon. Weather Rev.* **134** 2318–41
Hoogewind K A, Chavas D R, Schenkel B A and O'Neill M E 2020 Exploring controls on Tropical cyclone count through the geography of environmental favorability *J. Clim.* **33** 1725–45
Hsieh J-S and Cook K H 2007 A study of the energetics of African Easterly Waves using regional climate model *J. Atmos. Sci.* **64** 421–40
Iacono M J, Delamere J S, Mlawer E J, Shephard M W, Clough S A and Collins W D 2008 Radiative forcing by long-lived greenhouse gases: calculations with the AER radiative transfer models *J. Geophys. Res. Atmos.* **113** D13
Jiménez P A, Dudhia J, González-Rouco J F, Navarro J, Montávez J P and García-Bustamante E 2012 A revised scheme for the WRF surface layer formulation *Mon. Weather Rev.* **140** 898–918
Jonville T, Cornillault E, Lavaysse C, Peyrillé P and Flamant C 2024a Distinguishing north and south African Easterly waves with a spectral method: implication for tropical cyclogenesis from mergers in the North Atlantic *Q. J. R. Meteorol. Soc.* **151** e4909
Jonville T, Flamant C and Lavaysse C 2024b Dynamical study of three African Easterly Waves in September 2021 *Q. J. R. Meteorol. Soc.* **150** 2489–509
Kain J S 2004 The Kain–Fritsch convective parameterization: an update *J. Appl. Meteorol.* **43** 170–81
Klotzbach P J, Wood K M, Bell M M, Blake E S, Bowen S G, Caron L-P, Collins J M, Gibney E J, Schreck C J and Truchelut R E 2021 A hyperactive end to the Atlantic hurricane season October–November 2020 *Bull. Am. Meteorol. Soc.* **103** E110–28
Landsea C W 1993 A climatology of intense (or Major) Atlantic hurricanes *Mon. Weather Rev.* **121** 1703–13
Landsea C W, Bell G D, Gray W M and Goldenberg S B 1998 The extremely active 1995 Atlantic hurricane season: environmental conditions and verification of seasonal forecasts *Mon. Weather Rev.* **126** 1174–93
Lin I-I, Black P, Price J F, Yang C-Y, Chen S S, Lien C-C, Harr P, Chi N-H, Wu C-C and D'Asaro E A 2013 An ocean coupling potential intensity index for tropical cyclones *Geophys. Res. Lett.* **40** 1878–82
Lin Y-L, Farley R D and Orville H D 1983 Bulk parameterization of the snow field in a cloud model *J. Appl. Meteorol. Climatol* **22** 1065–92
Mekonnen A, Thorncroft C D and Aiyyer A R 2006 Analysis of convection and its association with African Easterly Waves *J. Clim.* **19** 5405–21
Muller C J and Held I M 2012 Detailed investigation of the self-aggregation of convection in cloud-resolving simulations *J. Atmos. Sci.* **69** 2551–65
Núñez Ocasio K M, Brammer A, Evans J L, Young G S and Moon Z L 2021 Favorable monsoon environment over Eastern Africa for subsequent Tropical cyclogenesis of African Easterly Waves *J. Atmos. Sci.* **78** 2911–25
Núñez Ocasio K M, Davis C A, Moon Z L and Lawton Q A 2024 Moisture dependence of an African Easterly Wave within the West African monsoon system *J. Adv. Model. Earth Syst.* **16** e2023MS004070
Pasch R J and Avila L A 1994 Atlantic Tropical systems of 1992 *Mon. Weather Rev.* **122** 539–48
Patricola C M, Chang P and Saravanan R 2016 Degree of simulated suppression of Atlantic tropical cyclones modulated by flavour of El Niño *Nat. Geosci.* **9** 155–60
Patricola C M, Saravanan R and Chang P 2018 The response of Atlantic Tropical cyclones to suppression of African Easterly Waves *Geophys. Res. Lett.* **45** 471–9
Peng M S, Fu B, Li T and Stevens D E 2012 Developing versus nondeveloping disturbances for tropical cyclone formation. Part I: North Atlantic *Mon. Weather Rev.* **140** 1047–66
Pérez-Alarcón A, Fernández-Alvarez J C, Sorí R, Nieto R and Gimeno L 2021 The combined effects of SST and the North Atlantic subtropical high-pressure system on the Atlantic basin tropical cyclone interannual variability *Atmosphere* **12** 329
Pytharoulis I and Thorncroft C 1999 The low-level structure of African Easterly waves in 1995 *Mon. Weather Rev.* **127** 2266–80
Russell J O H and Aiyyer A 2020 The potential vorticity structure and dynamics of African Easterly Waves *J. Atmos. Sci.* **77** 871–90
Russell J O H, Aiyyer A and Dylan White J 2020 African Easterly Wave dynamics in convection-permitting simulations: rotational stratiform instability as a conceptual model *J. Adv. Model. Earth Syst.* **12** e2019MS001706
Russell J O, Aiyyer A, White J D and Hannah W 2017 Revisiting the connection between African Easterly Waves and Atlantic tropical cyclogenesis *Geophys. Res. Lett.* **44** 587–95
Schwendike J and Jones S C 2010 Convection in an African Easterly Wave over West Africa and the eastern Atlantic: a model case study of *Helene Q. J. R. Meteorol. Soc.* **136** 364–96
Skamarock W C *et al* 2019 A description of the advanced research WRF model version 4 *NCAR Technical Note (No. NCAR/TN-556+STR)* (https://doi.org/10.5065/1dfh-6p97)
Skinner C B and Diffenbaugh N S 2014 Projected changes in African Easterly Wave intensity and track in response to

greenhouse forcing *Proc. Natl Acad. Sci. USA* **111** 6882–7
Thorncroft C and Hodges K 2001 African Easterly Wave variability and its relationship to Atlantic Tropical cyclone activity *J. Clim.* **14** 1166–79
Tyner B and Aiyyer A 2012 Evolution of African Easterly Waves in potential vorticity fields *Mon. Weather Rev.* **140** 3634–52
Walsh K 1997 Objective detection of Tropical cyclones in high-resolution analyses *Mon. Weather Rev.* **125** 1767–79
Wing A A, Emanuel K, Holloway C E and Muller C 2017 Convective self-aggregation in numerical simulations: a review *Surv. Geophys.* **38** 1173–97
Wong M L M and Chan J C L 2004 Tropical cyclone intensity in vertical wind shear *J. Atmos. Sci.* **61** 1859–76
Wu M-L C, Reale O and Schubert S D 2013 A characterization of African Easterly Waves on 2.5–6-day and 6–9-day time scales *J. Clim.* **26** 6750–74